



1 A machine learning approach to quantify meteorological drivers of 2 recent ozone pollution in China

3 Xiang Weng¹, Grant L. Forster^{1,2}, Peer Nowack^{1,3}

4 ¹ School of Environmental Sciences, University of East Anglia, Norwich, NR47TJ, UK

5 ² National Centre for Atmospheric Sciences, University of East Anglia, Norwich, NR47TJ, UK

6 ³ Grantham Institute – Climate Change and the Environment, Department of Physics, and the Data Science Institute, Imperial
7 College London, London SW7 2AZ, UK

8

9
10 Correspondence to: Xiang Weng (x.weng@uea.ac.uk)

11 **Abstract.** Surface ozone concentrations have been increasing in many regions of China for the past few years, in contrast to
12 policy-driven declines in other key air pollutants such as particulate matter. While the central role of meteorology in modulating
13 ozone pollution is widely acknowledged, its quantitative contribution remains highly uncertain. Here, we use a data-driven
14 machine learning approach to assess the impacts of meteorology on surface ozone variations in China for the years 2015 to
15 2019, considering the months of highest ozone pollution from April to October. To quantify the importance of various
16 meteorological driver variables, we apply non-linear random forest regression (RFR) and linear ridge regression (RR) to learn
17 relationships between meteorological variability and surface ozone in China, and contrast the results to those obtained with
18 the widely used multiple linear regression (MLR) and stepwise MLR. We show that RFR outperforms the three linear methods
19 when predicting ozone using only local meteorological predictor variables. This implies the importance of non-linear
20 relationships between local meteorological factors and ozone, which are not captured by linear regression algorithms. In
21 addition, we find that including non-local meteorological predictors can further improve the modelling skill of RR, particularly
22 for Southern China, highlighting the importance of large-scale meteorological phenomena for ozone pollution in that region.
23 Overall, RFR and RR are in close agreement concerning the leading meteorological drivers behind regional ozone pollution.
24 For example, we find that temperature variations are the dominant meteorological driver for ozone pollution in Northern China
25 (e.g., Beijing Tianjin Hebei region), whereas variations in relative humidity are the most important factor in Southern China
26 (e.g., Pearl River Delta). Variability in surface solar radiation modulates photochemistry but was not considered as such in
27 previous controlling factor analyses, and is found to be the most important predictor in the Yangtze River Delta and Sichuan
28 Basin regions. In general, our analysis underlines that hot and dry weather conditions with high sunlight intensity are strongly
29 related to high ozone pollution across China. This further validates our novel approach to quantify the central role of
30 meteorology. By contrasting our meteorological ozone predictions with ozone measurements between 2015 and 2019, we
31 estimate that almost half of the observed ozone trends across China might have been caused by meteorological variabilities on
32 average. We highlight that these insights are of particular importance given possible increases in the frequency and intensity
33 of weather extremes such as heatwaves under climate change.



34 1 Introduction

35 Surface ozone is an air pollutant that can induce severe harm to both human health and ecosystems (Lefohn et al., 2018;
36 Lelieveld et al. 2015). In the troposphere, it is primarily produced through photochemically induced reaction chains involving
37 volatile organic compounds (VOCs), nitrogen oxides (NO_x) and carbon monoxide (CO) (Monks et al., 2015; Jacob, 2000).
38 Over the last decade, Chinese policymakers have been successfully implementing air pollution control policies and strategies,
39 such as The Clean Air Action Plan in 2013 (Chinese State Council, 2013), to reduce harmful air pollutants. As a result, annual
40 mean concentrations of fine particulate matter (PM_{2.5}) have been reduced by 30% to 50% from 2013 to 2018 in China,
41 alongside significant decreases in emissions of ozone precursors such as NO_x and CO (Zhai et al., 2019; Zheng et al., 2018).
42 Despite decreasing trends in NO_x and CO, summertime surface ozone concentrations have been increasing from 2013 to 2019
43 at a rate of about 1.9 ppb yr⁻¹ on average across China, with a faster rate of 3.3 ppb yr⁻¹ in the North China Plain (Li et al.,
44 2020).

45 It is well-known that the effectiveness of ozone production is strongly dependent on the atmospheric chemical regime
46 (e.g., Squire et al., 2015, Archibald et al., 2020), in which ozone production is mainly controlled by the abundance of NO_x or
47 VOCs. Many urban and industrial regions in China have been identified and categorized as being within the VOC-limited
48 regime (Ou et al., 2016; Wang et al., 2017). Under these circumstances, surface ozone reductions may require tighter controls
49 on VOCs emissions together with continuous reductions in NO_x, while significant reductions in NO_x emissions without
50 simultaneous and adequate controls on VOCs could lead to increased ozone pollution in the short term (Wang et al., 2019),
51 which could largely explain the recent increases in surface ozone across China. Another factor might have been the large
52 reduction in PM_{2.5}, especially during the period of 2013 to 2017, because fewer particles could reduce the aerosol sink of
53 ozone-producing radicals such as hydroperoxyl (HO₂) (Li et al., 2019a). However, it is likely that this effect has become less
54 important as PM_{2.5} concentrations continue to decline (X. Chen et al., 2021; Li et al., 2019b).

55 In conjunction with the effects of changing ozone precursor emissions, the effect of meteorological conditions on ozone
56 concentrations should always be considered. Previous work has identified that ozone variations are strongly co-determined by
57 meteorological factors such as incoming solar radiation, temperature, humidity, atmospheric stagnation, and precipitation (e.g.,
58 Otero et al., 2018; Zhang et al., 2018; Lu et al., 2019a). For example, solar radiation is pivotal to the photochemical production
59 and destruction of ozone (Finlayson-Pitts and Pitts, 2000). Higher surface temperatures, and in general tropospheric
60 temperatures, change the chemical reaction rate of many ozone-relevant chemical reactions and will affect biogenic emissions
61 of VOCs such as isoprene and monoterpenes which are also important ozone precursors (Lu et al., 2019a; Doherty et al., 2013;
62 Guenther et al., 1993; Xie et al., 2008; Archibald et al. 2020). Work by Lu et al. (2019b) further indicated that hotter and drier
63 weather conditions were the main drivers for background ozone increase in 2017 in major city clusters of China. Similarly,
64 Ma et al. (2019) suggested that high biogenic VOCs emissions and meteorological conditions indicative of heatwaves such as
65 high temperature, low wind speed and no precipitation can elevate ozone pollution in the North China Plain (NCP).
66 Furthermore, studies by Wang et al. (2021) and Pu et al. (2017) also found enhanced ozone concentrations during heatwaves



67 in the Pearl River Delta (PRD) and Yangtze River Delta (YRD). Such links between meteorology and ozone pollution provide
68 clear evidence for the necessity to quantify the influence of meteorological factors or even climate change on ozone pollution
69 in China (e.g., Lu et al., 2019a; Meehl et al. 2018). Characterizing the major meteorological drivers behind ozone variations
70 in different regions of China will also be crucial for achieving effective mitigation of ozone pollution now and under future
71 changes in climate.

72 To quantify the importance meteorological drivers, previous studies such as Li et al. (2019a) and Han et al. (2020) adopted
73 stepwise multiple linear regression (MLR) to derive linear relationships between meteorological factors and measured surface
74 ozone concentrations across China. Both of these studies demonstrated the significant skill of stepwise MLR in modelling
75 ozone and in quantifying the driver-response relationships. Nevertheless, a key limitation of stepwise MLR or conventional
76 MLR is that these methods are not able to accurately capture non-linearity, which is a severe constraint given that non-linear
77 relationships between meteorological factors and ozone, e.g., between temperature and ozone, are to be expected (e.g., Pu et
78 al., 2017; Gu et al., 2020; Archibald et al., 2020). In addition, MLR can suffer from severe loss in predictive skill and reliability
79 in settings where a large number of (collinear) meteorological factors are considered as predictors (cf., the curse of
80 dimensionality in high-dimensional regression problems; Nowack et al., 2021; Bishop, 2006). Although the stepwise MLR
81 approach adopted by Li et al. (2019a) can overcome collinearity and overfitting to some extent because only a few predictors
82 that are particularly strongly influencing ozone concentrations are kept, it is inevitable that many relevant meteorological
83 factors will be excluded from the final MLR predictions using that approach.

84 In order to capture non-linear relationships between many meteorological factors and ozone and to overcome the potential
85 limitations of considering collinearity and high-dimensional settings in MLR, we will use a machine learning approach as the
86 next logical step to advance such controlling factor analyses of ozone pollution. Specifically, we will adopt random forest
87 regression (RFR) (e.g., Grange et al., 2018; Stirnberg et al., 2021) as a non-linear approach and contrast the results to a linear
88 statistical learning approach that is also robust in high-dimensional settings in the form of ridge regression (RR) (e.g., Nowack
89 et al., 2018). Both RFR and RR will also be compared with more conventional statistical methods such as MLR and stepwise
90 MLR.

91 Our paper is structured as follows. In Sect. 2, we describe the data used in this study and the modelling framework of the
92 two machine learning algorithms, namely, RFR and RR. In Sect. 3, the performances of RFR and RR will be discussed first
93 and then compared to those achieved with MLR and stepwise MLR. Afterwards, we summarize the most important
94 meteorological drivers for surface ozone as identified by RFR and RR. Finally, we conduct a trend analysis of recent surface
95 ozone changes in China, and use our method to estimate the contribution of meteorological effects.



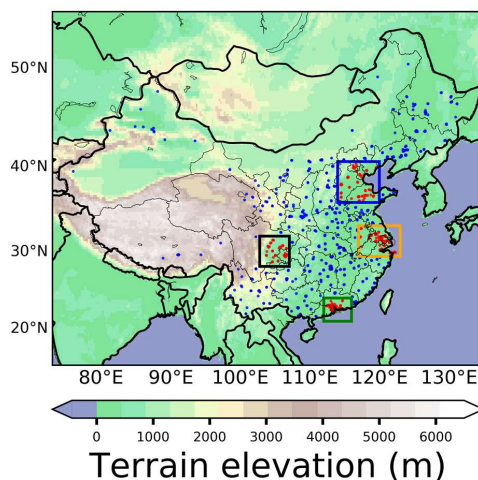
96 2 Methods

97 2.1 Surface ozone and meteorological data

98 The surface air quality measurement data used in this study were obtained from <https://quotsoft.net/air/> (Wang, X. L.,
99 2021; last accessed: 13 July 2021) which is a mirror of the data from the China Ministry of Ecology and Environment (MEE).
100 For the purposes of quantifying ozone pollution severity, we use the maximum daily 8-hour rolling mean (MDA8) ozone
101 calculated following the guidelines by the Ministry of Environmental Protection of People's Republic of China (MEP, 2012).
102 The calculation selects the maximum value from 8-hour rolling means of ozone for each station between 08:00 and 24:00 on
103 each day. To be considered, each station must have a valid 14 hours data record of 8-hour rolling means ozone within 08:00
104 to 24:00 on the respective day, otherwise MDA8 ozone is not calculated for that day. Previous studies (e.g., Li et al., 2020; Li
105 et al., 2019a; Han et al., 2020) have focused on ozone pollution during the boreal summer months i.e., June, July, and August
106 (JJA) as the season with the most frequent occurrence of extreme ozone episodes in China. In this work, we extend this analysis
107 period to include the months from April to October to account for the fact that the seasonality of ozone does not follow a
108 uniform pattern across China. For example, peak ozone concentrations are often found during autumn over the PRD region
109 (Gao et al., 2020; see Fig. S1 in the Supplementary Material). In addition, we further constrain our analysis to the period 2015
110 to 2019 to maintain greater consistency of the ozone data throughout our analysis period as the MEE included far fewer
111 measurement stations prior to 2015. In order to maintain consistency and reliability of all ozone data from stations within the
112 study period, only those stations with over 80% temporal coverage of MDA8 ozone data record in each year are selected. For
113 quality assurance of the data, we further examined each station's MDA8 ozone variation individually and noticed that
114 measurements from some stations appeared to show a less reliable data record than others. This was for example evident from
115 extended periods of non-fluctuating ozone levels (see Fig. S2), or from sudden unusual MDA8 spikes, usually followed by
116 periods of suppressed ozone variability (see Fig. S3). According to our best judgement, such abrupt changes or unrealistically
117 low variability are unlikely to reflect actual ozone pollution profiles. Data from stations that showed such unusual time
118 evolutions were excluded from our analysis as to avoid the inclusion of unrealistic artefacts. The list of stations that are not
119 used in this study is summarized in Table S1.

120 To study regional meteorological drivers of ozone, we distinguish four regions of particularly high population density
121 known as Beijing-Tianjin-Hebei (BTH, which is equivalent to north China plain), Yangtze River Delta (YRD), Pearl River
122 Delta (PRD) and Sichuan Basin (Sichuan), using definitions frequently used in previous studies (e.g., Li et al., 2019a; Han et
123 al., 2020). The boundaries of these four regions are adjusted to ensure that stations in each region have similar topography and
124 equivalent elevation. The four regions are also known as the target areas for air pollution reduction in Chinese government
125 plans (MEE; <http://www.mee.gov.cn/hjzl/dqhj/ckqzljzkyb/> last access: 1 December 2021; Li et al., 2019a). The locations of
126 stations within the four regions are indicated by red dots in Fig. 1.

127



128

129 **Figure 1. Elevation height (m) and locations of all ground-based stations and the four megacity cluster regions, BTH (blue box; 114°**
130 **E-120° E, 36° N-40.62° N), YRD (orange box; 117° E-123° E, 29.458° N-33.238° N), PRD (green box; 112° E-116° E, 21° N-24.111°**
131 **N), Sichuan Basin (black box; 102.8° E-107.061° E, 28.2° N-31.976° N). Red (blue) dots indicate locations of stations within (outside)**
132 **the four regions.**

133 For the meteorological data, we use the gridded ERA5 reanalysis product (Hersbach et al., 2020) available at
134 <https://cds.climate.copernicus.eu/> (last accessed: 11 November 2021). Specifically, we use hourly data for a total of 11
135 meteorological variables at 0.25°×0.25° spatial resolution, namely, temperature at 2 m (T2), boundary layer height (BLH),
136 mean sea level pressure (SLP), surface solar radiation downward (SSRD), relative humidity at 1000 hPa (RH), total
137 precipitation (TP), zonal wind at 10 m (U10), meridional wind at 10 m (V10), zonal wind at 850 hPa (U850hPa), meridional
138 wind at 850 hPa (V850hPa) and vertical velocity at 850 hPa (W850) for the same time period as for the ozone station data.
139 Then the MDA8 ozone data are spatially averaged within the dimensions of each ERA5 grid cell to obtain the best possible
140 spatial match between the station-based ozone data and the large-scale meteorological factor data.

141 The variables of T2, BLH, SLP, RH, TP, U10, V10 can also be found as predictors in the multi linear regression (MLR)
142 studies of Han et al. (2020) and Li et al. (2019a). Surface solar radiation downward (SSRD) is included in this study instead
143 of adding a cloud coverage term as done by Han et al. (2020) and Li et al. (2019a). Essentially, we consider SSRD to more
144 directly characterize the local photochemical environment for ozone production and loss than cloud coverage. Zonal and
145 meridional wind at 10 m may be important for dispersion of ozone's precursors on a local scale. Both zonal and meridional
146 wind at 850 hPa are adopted in this study in order to encompass the effect of transport of more polluted or cleaner air from
147 remote regions. Wind at 850 hPa is less likely to be affected by orography than wind at 10 m altitude, and it is thus better
148 suited for considering the effect of larger scale transport and dispersion. Additionally, we represent the role of vertical transport
149 of air masses by including vertical velocity at 850 hPa as another factor.



150 2.2 Data pre-processing

151 Prior to modelling ozone, we pre-processed the meteorological data by averaging the raw hourly data over different
152 periods each day and this process is summarised in Table 1. The averaging periods were not the same for all meteorological
153 variables. For example, T2, SSRD, SLP, RH, and W850 are averaged between local time (UTC+8:00) 06:00 to 18:00 on each
154 day. The average of these hours is sufficient to cover all daytime hours when ozone is photochemically produced from April
155 to October. Total precipitation is calculated as the sum of accumulated precipitation for all hours from 06:00 to 18:00. For
156 zonal and meridional wind at 10 m and 850 hPa, data are averaged over 06:00 to 12:00, which covers the main hours that may
157 have potential fresh emission of precursors and transport or dispersion of precursors or ozone. Boundary layer height (BLH)
158 is averaged over 00:00 to 12:00 for the consideration of both potential night-time emission of industrial activities when
159 boundary layer is still low and transportation emission during morning rush hours. Through this process, raw hourly
160 meteorological data can be converted to daily format, temporally matching with MDA8 ozone data.

161 **Table 1. Summary of the meteorological controlling factor variables and the respective times of day considered in their averages.**
162 **The motivation behind each selected time period is provided in the main text. Note: a positive zonal wind means westerly; positive**
163 **meridional wind means southerly; positive vertical velocity means downward motion.**

Acronyms	Names and units of variables	Average period
T2	temperature at 2 m (K)	06:00 to 18:00
SSRD	surface solar radiation downward (J m^{-2})	06:00 to 18:00
SLP	mean sea level pressure (Pa)	06:00 to 18:00
RH	relative humidity (%)	06:00 to 18:00
BLH	boundary layer height (m)	00:00 to 12:00
U10	zonal wind at 10m (m s^{-1})	06:00 to 12:00
V10	meridional wind at 10m (m s^{-1})	06:00 to 12:00
TP	total precipitation (m)	06:00 to 18:00 (sum)
U850hPa	zonal wind at 850hPa (m s^{-1})	06:00 to 12:00
V850hPa	meridional wind at 850hPa (m s^{-1})	06:00 to 12:00
W850	vertical velocity at 850hPa (Pa s^{-1})	06:00 to 18:00

164 Finally, both ozone data and meteorological data are deseasonalized. Specifically, for MDA8 ozone and the converted
165 daily meteorological variables, we first calculate 15-day moving window averages centered on the particular calendar date
166 from 2015 to 2019. We then take the difference between each day's MDA8 ozone or daily meteorological variables and these
167 15-day averages to obtain daily anomalies, creating smooth time series of deseasonalized MDA8 ozone and deseasonalized
168 meteorological variables.



169 **2.3 Machine learning methods for modelling MDA8 ozone**

170 To model the relationships between meteorological variables and MDA8 ozone concentrations in China, we use two
171 regression algorithms, a non-linear approach known as random forest regression (RFR) and a linear approach called ridge
172 regression (RR). Within our framework, the predictors are the deseasonalized meteorological variables from ERA5 and the
173 dependent variable is the deseasonalized ground-based MDA8 ozone. For RR, both the deseasonalized meteorological
174 variables and the deseasonalized ozone time series are standard-scaled (normalized to zero mean and unit standard deviation)
175 as to avoid an imbalance of factors in the regularization part of the RR cost function (Nowack et al., 2018).

176 Both RFR and RR have been extensively described elsewhere (e.g., Nowack et al., 2018; Grange et al., 2018; Mansfield
177 et al., 2020; Nowack et al., 2021) and it is beyond the scope of this study to provide an in-depth description. Briefly, RFR is
178 based on learning an ensemble of decision trees, where each individual tree splits data into groups until reaching certain pre-
179 set definitions for data ‘purity’ (Breiman, 2001; Grange et al., 2018). RR is a least-squares linear regression method augmented
180 by L2-regularization with the goal to avoid overfitting in high-dimensional regression settings, especially in regression
181 problems with strong collinearity (McDonald, 2009). Both RFR and RR are known to handle collinearity comparatively well
182 (e.g., Dormann et al. 2013), which is key given that many of meteorological variables such as temperature and solar radiation
183 are correlated with each other. To assess whether these two machine learning algorithms can improve the accuracy of ozone
184 modelling compared to conventional statistical methods, we will contrast our results to multiple linear regression (MLR) - that
185 may not be highly capable of handling collinearity and overfitting and stepwise MLR. For MLR, we simply adopt the same
186 modelling framework of RFR and RR; all 11 meteorological variables are ingested into MLR as predictors. For stepwise MLR,
187 we adopted a similar approach as Li et al. (2019a): we start with 11 deseasonalized meteorological variables as predictors in
188 MLR and remove one predictor at a time based on the smallest significance of the regression coefficient in each new subset of
189 predictors, until there are only 3 meteorological predictors left. These 3 predictors are considered to be important predictors
190 and are used in the final model of stepwise MLR for modelling deseasonalized MDA8 ozone.

191 **2.4 Training, testing and cross-validation in machine learning**

192 Supervised machine learning approaches such as the two algorithms we use here involve distinct training, validation and
193 testing phases to tune the relevant hyperparameters (explained in detail below) and to validate the skill of the resulting
194 predictive functions on new, unseen data not used in the training and tuning process (e.g., Bishop, 2006). During the training
195 phase, both predictors (i.e., deseasonalized meteorological variables) and dependent variable (i.e., deseasonalized MDA8
196 ozone) are available and each machine learning regression algorithm is fit to this dataset, assuming different combinations of
197 values for the hyperparameters of each algorithm. The best objective combination of hyperparameters is then found in the
198 validation step by predicting ozone values for a validation dataset not used at the training stage (e.g., for a different year in the
199 data record). During the testing phase, the trained and validated algorithm is used operationally to make new predictions for
200 ozone values given a new dataset for the meteorological variables as input to the machine learning function. These test set



201 predictions can then be used to measure the “out-of-sample” skill of the algorithm in predicting ozone pollution given certain
202 meteorological conditions. In this study, we split the 5-years of data (2015 to 2019) systematically into training/validation and
203 testing datasets one at a time and in a rotating fashion. Specifically, 4 of these 5 years are classified as training/validation data,
204 leaving 1 year for testing. To ensure that we are measuring the true predictive performance and relationships, our predictive
205 results and model evaluations are only conducted for the test data, which has not been used at the training and validation stages.
206 This process rotates until ozone data for each year have been assigned once as test data so that all 5 years of data can be
207 predicted by RFR and RR.

208 Machine learning regressions such as RFR and RR optimize their predictive performance by tuning certain sets of
209 hyperparameters. To determine the most suitable set of hyperparameters, we use a statistical cross-validation method. Initially,
210 we split the 5 years of data into 1 test year and 4 training/validation years. For cross-validation, the 4-year training/validation
211 set is further split into four folds (one year per fold). We then run a grid search over pre-defined combinations of
212 hyperparameters by training on three folds and predicting on the fourth fold in a classic 4-fold cross-validation procedure. We
213 finally select the best estimated set of hyperparameters on the basis of the average validation data prediction performance as
214 measured by the coefficient of determination (R^2 -score), and refit model coefficients using this set of hyperparameters for the
215 entire 4 years of training/validation data. We note that we avoid a ‘leave-one-out’ cross validation method as we expect
216 autocorrelation in our data (i.e., MDA8 ozone may share similarity in adjacent dates), which, intuitively, could lead to an
217 overestimate of our predictive skill if testing data immediately follows training data points.

218 The ranges of hyperparameters we search over for both RFR and RR are set as follows. For RFR, the maximum depth for
219 trees growing is iterated in a step of 1 from 8 to 15. Maximum percentage of features and maximum samples (with bootstrap
220 method) are set from 20% to 90% and 30% to 80% with 10% incremental step, respectively. Total tree number for the forest
221 is set at 200 as a compromise between model complexity and runtime. Optimizations further showed that the minimum samples
222 per leaf is best set to 3 in our RFRs so that we finally kept this value constant in our grid searches. In terms of RR, the
223 regularization strength is iterated over a range of 1 to 199 with incremental step of 2, which appeared to encapsulate the best
224 solution in each case. A detailed explanation of these hyperparameters for RFR and RR is for example provided in Nowack et
225 al. (2021).

226 2.5 Identifying and quantifying importance of meteorological drivers

227 Both RFR and RR can enable the identification of the most important meteorological drivers for MDA8 ozone and can
228 help to quantitatively evaluate their relative importance. For RFR, we here measure the importance of each meteorological
229 predictor through a metric called Gini importance. A greater Gini importance implies a greater influence of a particular
230 predictor (i.e., the deseasonalized meteorological variable) on the dependent variable (i.e., deseasonalized MDA8 ozone) (e.g.,
231 Menze et al., 2009; Zhao et al., 2019, Kuhn-Régner et al., 2021). Since we train the RFR five times for each set of 4-year
232 training/validation data, we average the Gini importance scores for each meteorological predictor across all five runs for our
233 final discussion below. For RR, similar to MLR, importance of each predictor is evaluated by the magnitude of each predictor’s



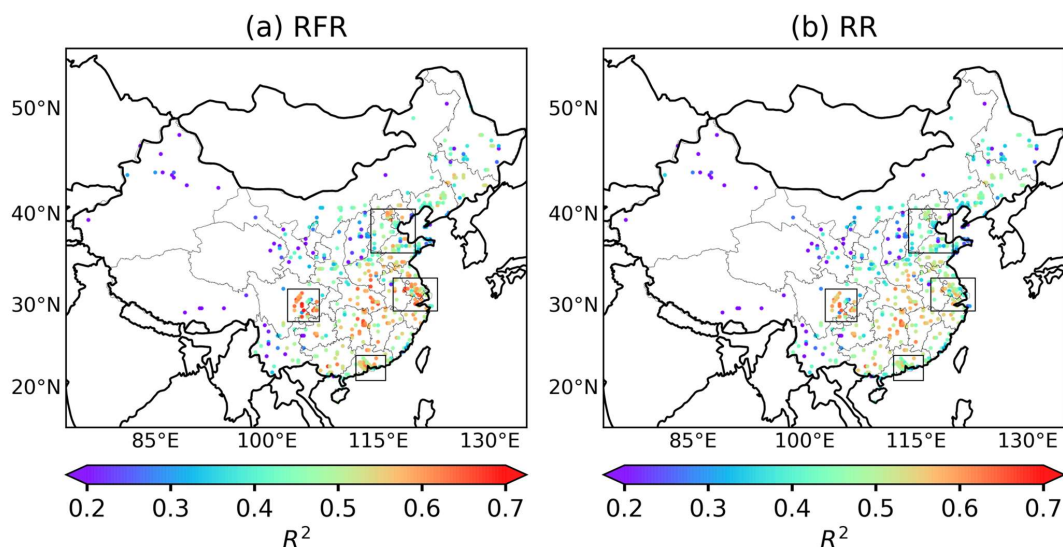
234 averaged slope (linear regression coefficient) across all 4-year training/validation datasets, which represents the linear effect
235 of each predictor onto ozone, given that all predictors are standard-scaled (see Sect. 2.3).

236 3 Results and discussion

237 3.1 Machine learning performances for modelling ozone using local meteorological predictors

238 It is important to first assess how well of these machine learning algorithms can model ozone by using only meteorological
239 variables as predictors. Therefore, we adopt the coefficient of determination (R^2) (i.e., the square of Pearson correlation
240 coefficient, R) as a standard metric for prediction performance on the deseasonalized MDA8 ozone data. As mentioned above,
241 to measure the true predictive skill of the machine learning functions, we only compare our predictions for out-of-sample test
242 data that are not used during training/validation stages against the deseasonalized measured MDA8 ozone data.

243 The predictors used by RFR and RR here are only the local meteorological variables, i.e., each ERA5 grid point's
244 meteorological variables are used as predictors to model averaged deseasonalized MDA8 ozone for that particular grid location.
245 The average prediction performance of RFR and RR by comparing predictions across all test years against the deseasonalized
246 measured MDA8 ozone data across China is illustrated in Fig. 2.



247
248 **Figure 2. Coefficient of determination (R^2) between deseasonalized observational MDA8 ozone and deseasonalized predicted values**
249 **in random forest regression (a) and ridge regression (b). The skill is only measured for the respective test datasets. Each dot**
250 **represents the center of the ERA5 grid location, within which station values for MDA8 ozone are averaged.**



251 Overall, the model performance of RFR generally surpasses the one of RR over most regions of China, with higher R^2
252 values in grid locations within the Sichuan Basin, YRD, PRD and other regions of southeast China. R^2 scores for RFR generally
253 range from 0.5 to 0.6 across China while RR reaches R^2 scores from 0.4 to 0.5. RFR and RR perform similarly over the central
254 region of BTH, while in the northern region of BTH (e.g., Beijing), R^2 values are still found to be higher in RFR than RR. The
255 averaged R^2 across all ERA5 grid locations within BTH, YRD, PRD, and Sichuan Basin is 0.46, 0.56, 0.53 and 0.57
256 respectively for RFR, which are all higher than the equivalent R^2 for RR (BTH: 0.41, YRD: 0.48, PRD: 0.47, Sichuan Basin:
257 0.53).

258 In order to examine whether RR can improve the model performance by being less sensitive to collinearity, we also
259 applied MLR with all 11 meteorological predictors and the stepwise MLR approach with the 3 most important meteorological
260 factors in the final MLR for comparison (see Sect. 2.3). Overall, stepwise MLR shows the worst performance with R^2 scores
261 ranging from 0.3 to 0.4 across China, with averaged R^2 scores in BTH, YRD, PRD and Sichuan Basin at 0.39, 0.45, 0.43 and
262 0.52, respectively (see Fig. S4b in Supplement for spatial distribution of R^2 scores). This suggests that the stepwise MLR
263 approach may carry a risk of not including all important meteorological predictors in the regression model. However, RR does
264 not show noticeable improvements over MLR, as evident from similar regionally averaged R^2 scores (see Fig. S4a), suggesting
265 that the problem of collinearity is still limited given the use of 11 meteorological predictors. The enhanced performance of
266 RFR compared to RR may therefore be attributed to RFR being able to model non-linear relationships between local
267 meteorological variables and ozone, indicating that a flexible machine learning approach such as RFR that can capture non-
268 linearity is more suitable to reflect relationships between local meteorological factors and ozone.

269 3.2 Predictive skill using additional non-local meteorological predictors

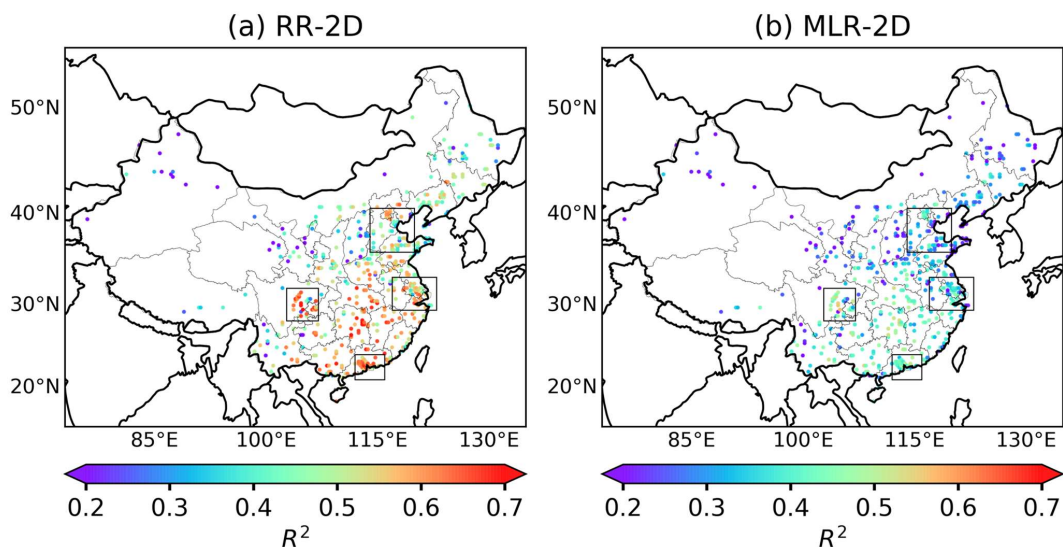
270 Meteorological phenomena usually belong into a larger spatial context. For example, high-pressure systems usually take
271 in a larger spatial domain, suppressing air flow in certain directions. Consequently, it seems intuitive that a meteorological
272 controlling factor framework for ozone might benefit from including additional non-local information in the regressions, i.e.,
273 if we were to consider surrounding meteorological context information that is not just limited to the predicted ozone grid point
274 in question (Ceppi and Nowack 2021).

275 We thus ran a second version of our controlling factor analysis in which we did not just include local values of
276 meteorological drivers, but additionally consider a spatially wider effect of meteorology on a two-dimensional (2D) domain
277 of meteorological variables. This is possible since both RR and RFR are less prone to collinearity and overfitting in high-
278 dimensional regression settings than simple non-regularized MLR approaches would be, meaning that the additional
279 information included in the regressions might well outweigh the cost of adding more predictors.

280 In detail, for each ozone target grid point, we include a meteorological context by adding each meteorological variable
281 within a $7.5^\circ \times 7.5^\circ$ rectangle domain around the center of this target grid point to the set of model predictors, i.e., all the
282 meteorological variables from the ERA5 $0.25^\circ \times 0.25^\circ$ grids within this $7.5^\circ \times 7.5^\circ$ rectangular domain are used as individual
283 predictors in the regression models. This adds potentially important information about the larger-scale meteorological situation



284 to our predictions, but also significantly increases the dimensionality (number of predictors) of our regression problem and
285 increases the number of collinear predictors. Indeed, we find that through the additional L2-regularization in RR with 2D
286 expansion (denoted as RR-2D), its predictions by far outperform its MLR-2D equivalent which now suffers from severe
287 overfitting (compare R^2 scores in Fig. 3a and 3b). Noteworthy, with the increase of dimensionality in RR-2D, the regularization
288 strength now is adjusted to larger values starting from 10^3 to 10^9 with a factor of 1.42 incremental increase at each step, which
289 is much higher than the regularization strength set in RR with only local predictors. Such a large increase of range is due to the
290 consideration of adding large number of meteorological predictors within the 2D domain, and it ensures that the best solution
291 with the most suitable regularization strength for each run can be well covered within this range. The overall R^2 scores for RR-
292 2D ranges from 0.5 to 0.6 while R^2 in MLR-2D ranges from 0.3 to 0.4; MLR-2D is overall worse than MLR with only local
293 meteorological predictors in terms of R^2 . It is well-known that RFR may not be as effective at handling multi-collinearity in
294 very high dimensional settings as RR (e.g., Dormann et al., 2013) and its training time also increases exponentially with the
295 number of predictors. We thus only ran RFR with 2D expansion (denoted as RFR-2D) for the southern Chinese PRD region,
296 where we found a particularly large R^2 -score improvement after including non-local predictors in RR-2D ($R^2=0.60$) as
297 compared to local RR ($R^2=0.47$), and even non-linear local RFR ($R^2=0.53$). These results highlight the apparent importance
298 of large-scale meteorological phenomena in this region. However, we find that RFR-2D improves the average R^2 score (0.57)
299 relative to RR and RFR with only local predictors, but does not perform better than RR-2D.



300

301 **Figure 3** Coefficient of determination (R^2) between deseasonalized observational MDA8 ozone and deseasonalized predicted values
302 of MDA8 ozone in ridge regression (RR) with 2D expansion (a) and MLR with 2D expansion (b).



303 For clarity, Table 2 summarizes the averaged R^2 in each region by all machine learning methods including RFR, RR,
304 MLR, stepwise MLR, RR-2D, MLR-2D and RFR-2D. In summary, RFR and RR-2D are overall the two machine learning
305 algorithms with highest R^2 in these four regions, while MLR and RR are equivalent.

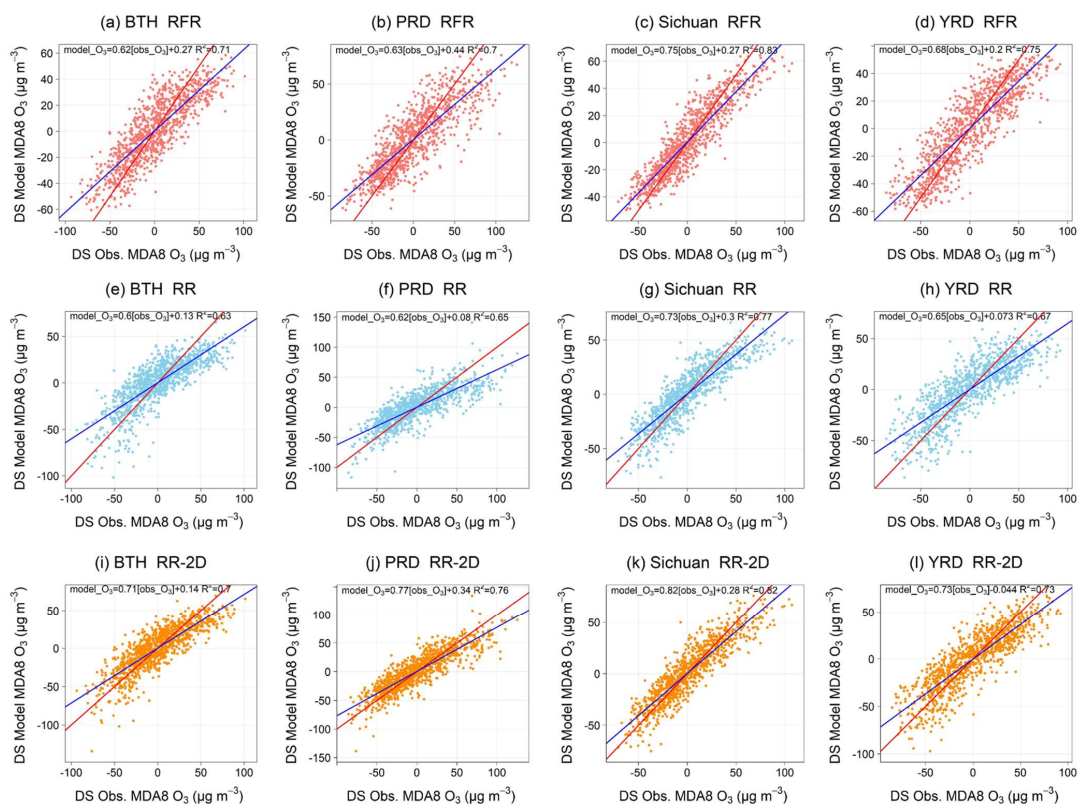
306 **Table 2. Averaged R^2 in the four regions by different machine learning algorithms, namely RFR, RR, MLR and stepwise MLR with**
307 **only local meteorological predictors, RR-2D, MLR-2D with additional two-dimensional (2D) non-local meteorological variables and**
308 **RFR-2D which is only conducted for PRD region. In general, with only local meteorological variables, RFR performs the best with**
309 **highest averaged R^2 in four regions. RR-2D and RFR-2D show improvement over PRD region compared to RFR.**

Method	BTH	YRD	PRD	Sichuan
RFR	0.46	0.56	0.53	0.57
RR	0.41	0.48	0.47	0.53
MLR	0.41	0.48	0.47	0.53
stepwise MLR	0.39	0.45	0.43	0.52
RR-2D	0.47	0.54	0.60	0.58
MLR-2D	0.31	0.35	0.42	0.43
RFR-2D	-	-	0.57	-

310 3.3 Regionally averaged prediction skill

311 In order to assess the performance of the algorithms in modelling regional average ozone, we further compared our
312 regionally-averaged machine learning predictions by RFR, RR and RR-2D against observations for each of the four selected
313 regions in China (Fig. 4), whereas previously we compared regional averages based on predictions for individual grid points
314 whose R^2 scores were subsequently averaged within each region. For this purpose, we averaged all $0.25^\circ \times 0.25^\circ$ grid point
315 observations and model results within each region first and then compared the resulting time series for each test dataset directly.
316 The results of regional averaged predictions and observations for each region are shown in Figure 4, where the goal for the
317 predictions is to fall as close as possible onto the 1:1-line, in combination with a high R^2 -score (i.e., square of Pearson
318 correlation, R). With only local meteorological predictors, RFR still outperforms RR regarding both the coefficient of
319 determination (R^2 , same calculation method as above) and slope (closer to 1) in all four regions. This can likely be attributed
320 to the ability of RFR to capture non-linearity as well.

321 Using this calculation method, regional R^2 are much higher; for RFR, regional R^2 in BTH, YRD, PRD and Sichuan Basin
322 is 0.71, 0.75, 0.7 and 0.83, since each grid is more prone to the effect of local emissions and related local uncertainties as
323 regional average can factor out the local effects (i.e., emissions and uncertainties) to some extent. For instance, stations that
324 are located relatively close to emission source may be more influenced by NO titration effect which may lower ozone level
325 (Sillman, 1999). This effect can be more significant in some urban areas (Li et al., 2017) or stations affected by fresh emission
326 of NO from power plants (X. Zhang et al., 2021). On the other hand, nearby emission of precursors may also be the dominant
327 factor in driving ozone in regular weather condition. Given both of these effects, ozone production in these stations may be
328 less sensitive to meteorological drivers but more influenced by local emissions.



329

330 **Figure 4 (a)-(d) Comparison of regional averages of deseasonalized MDA8 ozone between model predictions and observations for**
331 **RFR, (e)-(h) RR and (i)-(l) RR-2D. Linear fits between predicted and observed data are indicated by blue lines; red lines are the**
332 **ideal 1:1 lines. The values for both models and observations are averaged over all ERA grid points in each region. Each graph**
333 **contains information of the linear regression with slope and R² score (i.e., square of Pearson correlation, R).**

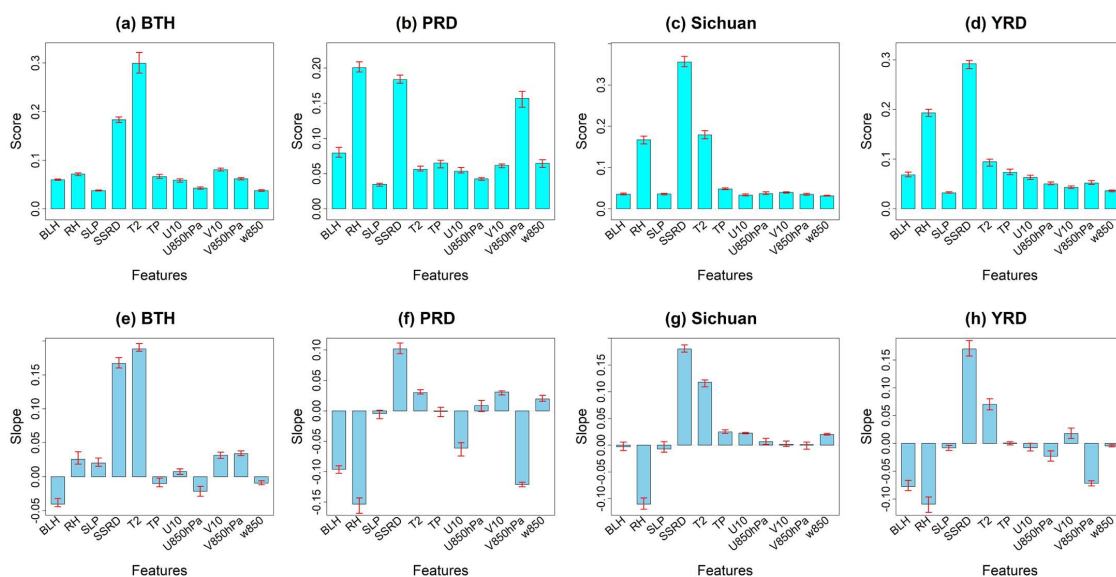
334 In summary, all three machine learning methods show clear skill in modelling ozone variability driven by meteorological
335 variables. However, similar to results by Han et al. (2020), all linear fits in all regions for both RFR and RR have slopes lower
336 than 1, suggesting a systemic underprediction of ozone for the highest observed ozone levels (higher than the deseasonalized
337 zero mean) and overpredictions of ozone for low ozone pollution regimes (lower than the deseasonalized zero mean). As
338 previously mentioned, such a mismatch may - at least to a degree - arises from non-meteorological factors such as the effect
339 of precursor emissions, which are not taken into account here. Although regionally averaged prediction skill is less affected
340 by local emissions, it will not be completely free from such effects. However, the increase of the magnitude of the slopes in
341 RR-2D with closer to 1 also suggests that considering non-local meteorological variables may help improve the performance
342 of ozone pollution controlling factor analyses, even if non-linearity is not intrinsically taken into account.



343 3.4 Quantifying the importance of meteorological predictors

344 We next aim to quantify how important each local meteorological predictor is for ozone pollution across China. For RR,
345 we use the regression slope as a standard metric to measure how important of each the meteorological predictor on ozone
346 pollution. A large positive value for the slope (regression coefficient) of a meteorological predictor indicates that the predictor
347 has a strong positive effect on ozone levels and vice versa. Since each of the 4-year training data is learned independently, we
348 will show averaged results. For RFR, we measure each predictor's importance through Gini importance (see Sect. 2.5). The
349 highest absolute value for both the RR slope or RFR Gini importance is interpreted as the most important meteorological driver
350 variable identified through our data-driven learning procedure. Note that Gini importance only allows to measure relative
351 influences of predictor variables on ozone variability, but not the sign of the influence, i.e., a high value of Gini importance
352 score is not able to determine whether the predictor has positive or negative effect on ozone.

353 The Gini importance scores estimated by RFR and the slopes learned by RR for each region are shown in Fig. 5. Both
354 Gini importance scores and slopes are initially estimated for every ERA5 grid location within each region and then averaged
355 across the entire region and across all five learned regression functions.



356

357 **Figure 5 (a)-(d) Average Gini feature importance scores of each meteorological variable for RFR in each region. (e)-(h) Average**
358 **slopes of each meteorological variable for ridge regressions in each region. The red bars indicate the range of importance**
359 **scores/slopes found across the five regression models learned to predict the left-out test years.**

360 In general, both RFR and RR show good agreement in terms of identifying the dominant meteorological drivers for each
361 region. Temperature at 2 m is found to be the most important meteorological driver for ozone in BTH, followed by surface



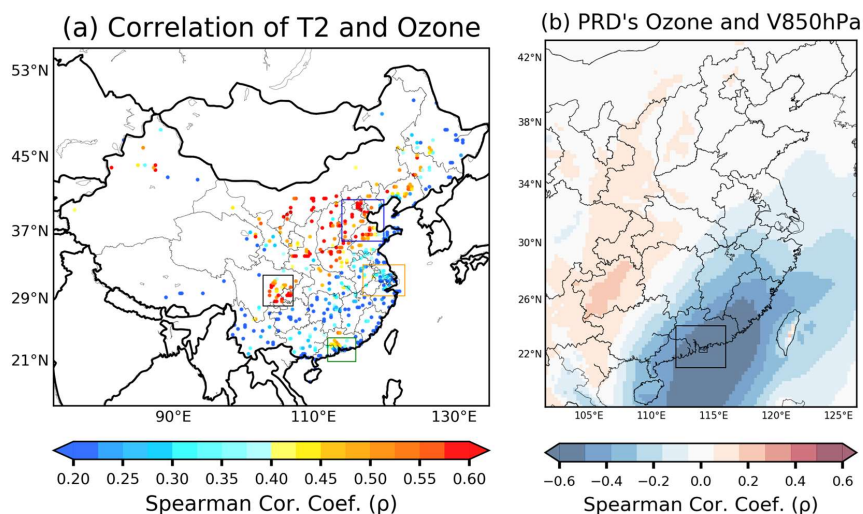
362 solar downward radiation, albeit the relative difference between these two variables differs more clearly for RFR, which might
363 be caused by non-linearity in the ozone-temperature relationship (Supplementary Fig. S5). Temperature was also identified as
364 the most important meteorological variable in BTH by Li et al. (2019a) using MLR. Moreover, a more pronounced positive
365 correlation between daily maximum temperature and MDA8 ozone is found in northern regions of China (Fig. 6a), which is
366 consistent with the findings of these two machine learning algorithms. Biogenic emissions can be intensified during heatwaves
367 in BTH, leading increased ozone (Ma et al., 2019). Additionally, high temperature conditions may also lead to the
368 intensification of certain anthropogenic emissions such as solvent evaporation. A detailed emission inventory in 2013 for BTH
369 shows that solvent use makes the highest contribution to NMVOC emissions at 46.7% in the industry sector (Qi et al., 2017).
370 Song et al. (2019) conducted a one-year observation (from April 2016 to March 2017) of VOCs at an urban site in BTH and
371 found that biogenic emissions and solvent use can make major contribution to ozone formation, and the concentrations of the
372 reactive VOCs species derived from these sources are found to have a positive correlation with temperature. In summary, with
373 higher temperature, biogenic emissions and solvent evaporation may be more intense, which may be one of the underlying
374 causes for elevated ozone pollution in BTH with higher temperatures.

375 For both YRD and Sichuan, surface solar radiation is most important determinant of ozone variations, with RR slopes
376 again indicating the expected positive relationship between sunny, clear-sky days and high ozone pollution. Solar radiation is
377 also found to be important in BTH, PRD by RFR and RR, suggesting its consistent importance across China. The importance
378 of solar radiation should be given more consideration in assessing the effect of meteorological drivers on ozone pollution.
379 High solar radiation stimulates the photochemical environment, which has been suggested as one of the key mechanisms in
380 YRD by Pu et al. (2017). From a large-scale meteorological point of view, such clear-sky conditions in YRD that may enhance
381 severe ozone pollution in this region are modulated by the western Pacific subtropical high (WPSH) (Shu et al., 2016; Chang
382 et al., 2019; Shu et al., 2020). In the Sichuan Basin, with complex terrain that can complicate atmospheric circulation, ozone
383 pollution is often associated with the occurrence of high-pressure systems associated with clear-sky conditions and high
384 temperatures (Ning et al., 2020), which is also identified by both RFR and RR.

385 A distinct difference in the weather-ozone coupling relationships is found for PRD, where relative humidity is the
386 dominant meteorological driver. Specifically, a negative slope of RH in RR suggests that drier conditions are strongly favorable
387 for peak ozone concentrations in PRD. As one of many possible effects of humidity, ozone may be more destroyed through
388 the photolysis reaction of $O_3 + h\nu \rightarrow O(^1D) + O_2$ as $O(^1D)$ can subsequently react with H_2O , forming OH through reaction of
389 $O(^1D) + H_2O \rightarrow 2OH$, which will be enhanced in environments with high humidity (Wang et al., 2013; Young et al., 2013).
390 In addition, despite more OH may be available given high humidity, OH can react with NO_2 , forming HNO_3 in highly NO_x -
391 polluted regions, which ultimately leading to less efficient O_3 formation by competing with the oxidation of VOC and CO with
392 OH (Lu et al., 2019a). The negative correlation between humidity and ozone in PRD region has been identified by previous
393 studies (W. Zhang et al., 2021; Yang et al., 2021; Hua et al., 2008), and the high humidity environment in southern China may
394 be the result of moisture marine air masses transported from tropical region, South China Sea and western Pacific (W. Zhang
395 et al., 2021; Ding and Chen, 2005). For a non-linear learning framework using RFR, the second most important meteorological



396 driver in PRD is again the level of surface solar radiation. Interestingly, meridional wind at 850 hPa is key to ozone occurrence
397 in PRD, and it is negatively correlated with average MDA8 ozone. More generally, the regional average of MDA8 ozone in
398 PRD is negatively correlated with meridional wind at 850hPa from South China Sea (Fig. 6b), indicating strong marine air
399 inflow may have a significant cleaning and dispersion effect on PRD ozone and its precursors. Furthermore, the negative
400 correlation also expands to the northeast areas to the PRD, suggesting lower ozone in PRD given strong southerly wind in
401 these areas, which may hinder the transport of ozone and its precursors to PRD. This finding is consistent with the backward
402 trajectories and numerical modelling analysis by Qu et al. (2021).



403

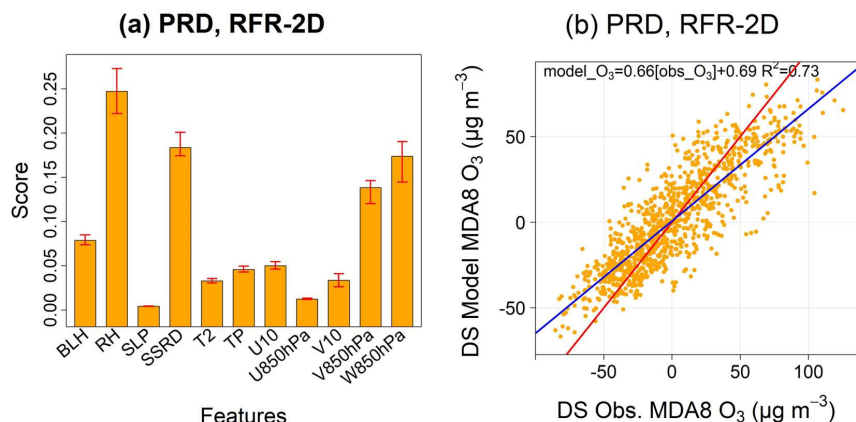
404 **Figure 6** (a) Spearman correlation between daytime (06:00 to 18:00) averaged temperature at 2 m and MDA8 ozone from 2015 to
405 2019 from April to October. (b) Correlation coefficients between regional average of MDA8 ozone in PRD and daytime meridional
406 wind at 850hPa at each ERA5 grid point from April to October of 2015 to 2019. A positive value of meridional wind indicates
407 southerly wind.

408 Additionally, previous studies (Jiang et al., 2015; Z. Chen et al., 2021; Qu et al., 2021; Wei et al., 2016) also indicate the
409 importance of vertical downward transport of ozone in southern region of China due to typhoons. The geographical location
410 and the intensity of typhoons can modulate the level of ozone in PRD; when typhoons are located relatively far away from
411 PRD during their development period, ozone can be elevated by downward movement of air masses, atmospheric stagnation
412 and lower planetary boundary layer height (Z. Chen et al., 2021), leading to suppressed dispersion of ozone and its precursors
413 before typhoon landing (Jiang et al., 2015; Z. Chen et al., 2021).

414 To illustrate the importance of such larger-scale meteorological effects on ozone pollution in PRD, we refer back to our
415 two-dimensional (2D) approach for RFR in PRD region first introduced and described in Sect. 3.2. We show the Gini feature
416 importance scores for this 2D domain approach in Fig. 7(a). Since we have multiple feature importance for each meteorological



417 variable in this set-up (i.e., one for each grid point in the 2D predictor domain), we sum up Gini scores for all grid points within
418 the expanded domain for each meteorological variable; and this summed value is denoted as the importance for that particular
419 meteorological variable. As illustrated in Fig. 7 (a), the relative feature importance of vertical velocity at 850hPa (w850)
420 increases compared to RFR using only local predictors (see Fig. 5b), likely reflecting the larger-scale influences of downward
421 transport of air masses in PRD region. Other key meteorological drivers (RH, solar radiation and meridional wind at 850hPa)
422 remain in a similar order to what was identified by purely local regressions. The model performance is slightly improved by
423 adding the 2D information with an increase of R^2 to 0.73 (from 0.70) in comparison to original RFR without 2D expansion.
424 However, we note that there appears to be a trade-off between the inclusion of non-linear relationships using RFR and
425 collinearity in high dimensions. Indeed, we find that the R^2 in RFR-2D for PRD region (see Fig. 7b) is still slightly less than
426 the R^2 using RR-2D (0.76) and the predictions from RR-2D are closer to observations with less deviations at both high and
427 low ozone value predictions (see Fig. 4j), suggesting that RR is better at handling the dimensionality increase of predictors,
428 which now slightly outweighs the importance of non-linearity in high dimensions.



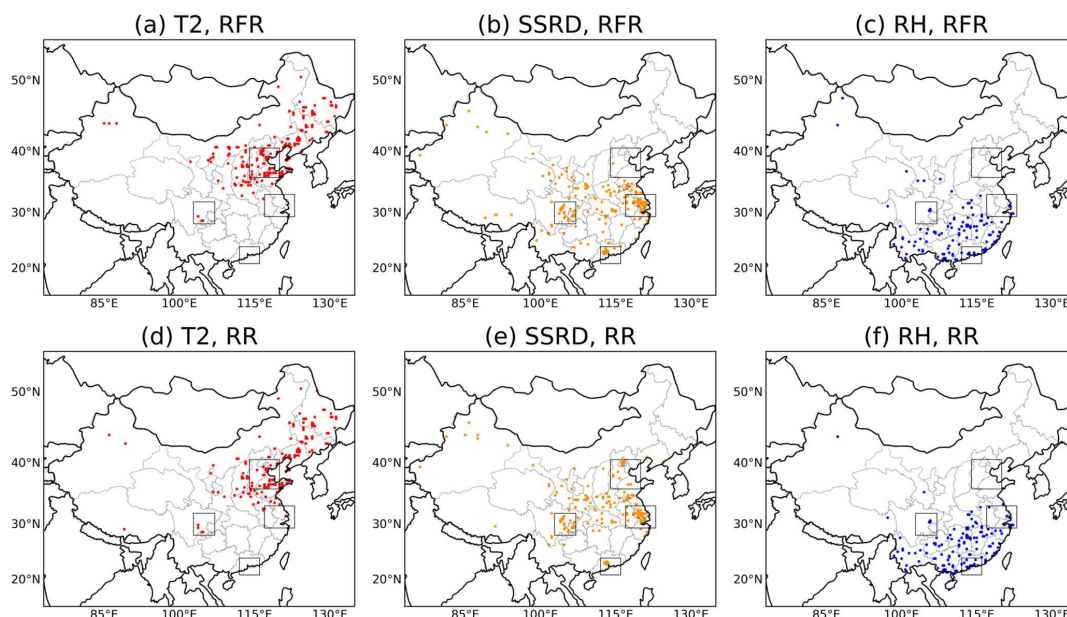
429

430 **Figure 7. (a) Average PRD Gini feature importance score of each meteorological variable if each regression includes non-local**
431 **predictors within a 7.5° longitude × 7.5° latitude grid; the bar representations are consistent with Figure 5. (b) Linear fit between**
432 **model prediction and observation in PRD using this 2D approach is drawn in blue line, red line equals the ideal 1:1 line.**

433 Across China, we found that there is a consistency in identification of the most important meteorological drivers by RFR
434 and RR. Temperature, solar radiation and RH are the three most commonly found most important meteorological drivers across
435 China, and the spatial distributions of these drivers are presented in Fig.8. Overall, there is a distinctive distribution pattern of
436 the 3 major meteorological drivers in China. Temperature at 2 m is dominant over northeast China, covering BTH and expand
437 to the norther region of China. Most areas in mid-latitude region of China including East China (e.g., YRD) and Sichuan Basin
438 show solar radiation as the main meteorological driver for ozone. The dominance of solar radiation gradually expands
439 northward and southward from this region while being overtaken by temperature in the north and relative humidity in the south.



440 Ozone in southern China is primarily driven by relative humidity. Such a distinctive spatial distribution of meteorological
441 drivers may be related to the characteristics of regional climatology. For instance, as previously described, regions in the
442 southern China such as PRD are more influenced by the moisture air masses, leading to the importance of humidity surpassing
443 temperature and solar radiation. While the relative drier northern regions do not have such a changeable humidity, making
444 temperature and solar radiation the key meteorological factors driving ozone.



445
446 **Figure 8 (a)-(c) Most important meteorological drivers at each grid location from April to October of 2015 to 2019 as identified by**
447 **Gini importance using RFR. (d)-(f) The same but using absolute magnitudes for the slopes of RR. Variables as labelled. Relative**
448 **humidity (RH) dominates in the South and South-East, surface solar downward radiation (SSRD) primarily in the Central China**
449 **and Eastern China, and temperature at 2 m (T2) in the North and North-East China.**

450 3.5 Anthropogenic and meteorological contributions to surface ozone trends from 2015 to 2019

451 Finally, we explore how our new machine learning approach could be used to study the quantitative influence of
452 meteorology on historical ozone variability and trends in China. To facilitate a comparison to previous work, we use a similar
453 method as Li et al. (2020) to establish estimates for observed surface ozone trends in China. We note that our exercise is
454 somewhat limited by the slightly shorter period considered here, i.e., from 2015 to 2019, instead of starting from earlier years.
455 Given this very short period, we are aware that any long-term trend analysis is explorative and has to be interpreted carefully,
456 as will also become evident from low statistical significance in many detected trends. We nevertheless attempt such an analysis
457 to demonstrate how our method can be used in such contexts and to also evaluate if any statistically significant trends are



458 robust after accounting for meteorological influences. After all, as we have demonstrated above, we can quantify such
459 influences with greater skill than using simple MLR methods applied previously.

460 For trend analyses, we first convert MDA8 ozone concentrations from mass concentrations ($\mu\text{g m}^{-3}$) to volume mixing
461 ratios (ppbv). We then average MDA8 ozone over April to October or summertime for each year for both observational data
462 and model results predicted by our three best-performing controlling factor regressions (RFR, RR and RR-2D). The predictions
463 can be considered as a quantitative estimate for the influence of meteorology on the ozone record during the study period. The
464 residual (true ozone signal minus meteorological predictions) will for example be mainly reflective of anthropogenic
465 contribution but will also inevitably contain some uncertainties related to the accuracy of the machine learning algorithms in
466 modelling ozone.

467 Table 3 summarizes the regionally averaged observed trends from 2015 to 2019, which is estimated by ordinary linear
468 regression in the four regions. We additionally list our meteorologically estimated trends and the residual trends. Overall, the
469 three machine learning methods provide very similar estimates of meteorologically driven trends in BTH, YRD and Sichuan
470 Basin, while we find indications that the meteorologically driven trend in PRD may be underestimated by only using local
471 meteorological factors; using RR-2D we estimate a meteorologically driven trend of 0.84 ppbv a^{-1} during April to October
472 from 2015 to 2019, while RFR and RR with only local meteorological predictors provide estimates of 0.1 ppbv a^{-1} and 0.003
473 ppbv a^{-1} , respectively. Given the better prediction skill in RR-2D for this region (see Table 2 and Fig. 4), this further suggests
474 the importance of spatial meteorological phenomena for ozone trend attribution exercises in the PRD region.

475 In terms of the raw observed trends, both BTH and PRD show significant increases in ozone pollution ($p < 0.05$) during
476 April to October from 2015 to 2019. We note that the observed trend in PRD is only significant if the months April to October
477 are considered, whereas there is no significant trend ($p = 0.93$) if only examining months in summertime (JJA). This may be
478 attributed to the ozone's seasonality in PRD where highest ozone pollution occurs during autumn and the particularly high
479 ozone anomaly during September and October in 2019 (Fig. S6b). We underline that anthropogenic contribution (i.e., the
480 residual) may be overestimated in PRD if only local meteorological factors are considered, given that both residuals of RFR
481 and RR increase compared to RR-2D. For BTH, the positive ozone trend is found to be more significant during summertime
482 at 3.20 ppbv a^{-1} ($p = 0.05$) than if the whole April to October period (2.53 ppbv a^{-1} , $p < 0.05$) is considered. Moreover, estimated
483 by RFR, the meteorologically driven trend in BTH is also higher at 0.74 ppbv a^{-1} ($p < 0.1$) during summertime than if the whole
484 April to October period is considered (0.45 ppbv a^{-1} ; $p = 0.14$). The April-to-October residual trends in BTH estimated by all
485 three algorithms are all greater than 2 ppbv a^{-1} ($p < 0.1$), indicating an elevated importance of anthropogenic drivers in BTH.
486 There are no significant observed trends in YRD and Sichuan. However, meteorological factors in both of these regions appear
487 to make a stronger influence according to RFR, RR and RR-2D. In terms of regional averages, all three of the machine learning
488 algorithms also agree on meteorologically driven negative trends in Sichuan while positive trends are found for YRD.

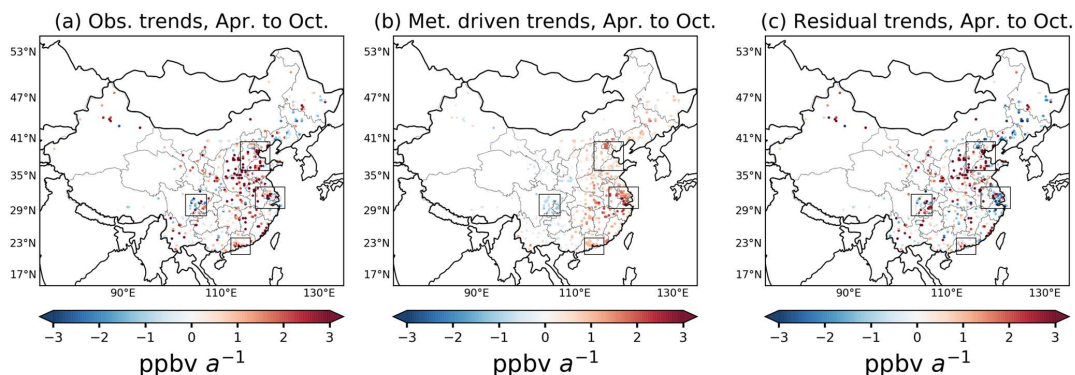
489 **Table 3. Observational, meteorological and residual trends of regional averaged MDA8 ozone (ppbv a^{-1}) from 2015 to 2019 for both**
490 **April to October and Northern Hemisphere summertime (June, July, August). Values within the brackets are the p values for each**
491 **trend. Trends and p values are in bold given p values smaller than 0.1.**



Method	Regions	2015-2019 Apr. to Oct.			2015-2019 Summer		
		Observed	Meteorological	Residual	Observed	Meteorological	Residual
RFR	BTH	2.53 (0.02)	0.45 (0.14)	2.08 (0.04)	3.2 (0.05)	0.74 (0.08)	2.46 (0.06)
	PRD	1.18 (0.02)	0.1 (0.88)	1.08 (0.08)	-0.12 (0.93)	-0.75 (0.14)	0.64 (0.58)
	Sichuan	-0.34 (0.57)	-0.75 (0.04)	0.42 (0.32)	0.01 (0.99)	-0.91 (0.34)	0.92 (0.11)
	YRD	0.87 (0.36)	1.38 (0.04)	-0.51 (0.48)	1.53 (0.15)	1.35 (0.07)	0.17 (0.81)
RR	BTH	2.53 (0.02)	0.37 (0.17)	2.17 (0.03)	3.2 (0.05)	0.54 (0.18)	2.66 (0.05)
	PRD	1.18 (0.02)	0.003 (0.997)	1.18 (0.09)	-0.12 (0.93)	-1.13 (0.11)	1.01 (0.39)
	Sichuan	-0.34 (0.57)	-0.84 (0.05)	0.51 (0.18)	0.01 (0.99)	-0.84 (0.4)	0.85 (0.06)
	YRD	0.87 (0.36)	1.41 (0.04)	-0.54 (0.43)	1.53 (0.15)	1.38 (0.09)	0.14 (0.86)
RR-2D	BTH	2.53 (0.02)	0.47 (0.35)	2.06 (0.09)	3.2 (0.05)	0.7 (0.33)	2.5 (0.11)
	PRD	1.18 (0.02)	0.84 (0.31)	0.34 (0.58)	-0.12 (0.93)	-0.33 (0.62)	0.21 (0.81)
	Sichuan	-0.34 (0.57)	-0.86 (0.02)	0.52 (0.25)	0.01 (0.99)	-0.68 (0.46)	0.69 (0.21)
	YRD	0.87 (0.36)	1.45 (0.08)	-0.58 (0.47)	1.53 (0.15)	1.63 (0.02)	-0.10 (0.91)

492

493 Finally, we aim to calculate trends on a ERA5 grid-by-grid point basis. Although RFR, RR and RR-2D all show significant
 494 skill in modelling ozone across China, RR-2D exhibited particularly increased predictive skill in southern China. Therefore,
 495 for assessing meteorologically-driven trends of MDA8 ozone across all ERA5 grid locations in China, we will only be
 496 examining the results for RR-2D. Fig. 9 shows trends during April to October from 2015 to 2019 across China. Overall, the
 497 observed average trend across China is 1.1 ppbv a⁻¹. The meteorologically driven trend of RR-2D gives the average at 0.5 ppbv
 498 a⁻¹ across China, which is around 45% of the total trend. From Fig. 9 (a), most regions in eastern China show a positive trend
 499 and the magnitudes of increase are more apparent in areas within and nearby BTH, where the ozone pollution increased at an
 500 average rate of 2.6ppbv a⁻¹ across all grids within BTH. We find that the positive trend in those particular regions may be less
 501 driven by meteorological factors but indeed might be the result of anthropogenic influences on air pollution (e.g., Liu and
 502 Wang, 2020). In YRD, meteorologically driven positive trends are in general the highest in eastern China (average at 1.47
 503 ppbv a⁻¹ across all grids in YRD), which is close to the regional averaged result by RR-2D (1.45 ppbv a⁻¹, $p=0.08$) in Table 3.
 504 Observed trends in Sichuan are a mixture of both increases and decreases, but meteorologically driven trends are all negative
 505 within this region. In PRD, meteorological factors likely played a more central role in driving the recent positive trends in
 506 ozone pollution according to our analysis.
 507



508

509 **Figure 9** Trends of MDA8 ozone during April to October from 2015 to 2019. (a) shows the observed trend. (b) shows the mean
510 meteorologically driven trends of MDA8 ozone according to RR-2D. (c) shows the residual (approximating anthropogenic effects).
511 The trends are estimated by the slope of an ordinary linear regression fitting each year's April-October MDA8 average ozone values
512 from 2015 to 2019.

513 **4 Conclusion**

514 Ozone pollution in China can be strongly influenced by meteorological conditions. This study examines the major
515 meteorological drivers for ozone pollution across China during months with particularly high ozone pollution (i.e., April to
516 October, from 2015 to 2019) using a controlling factor framework and two machine learning algorithms, namely random forest
517 regression (RFR) and ridge regression (RR).

518 The results obtained with RFR and RR are also compared with conventional approaches i.e., multiple linear regression
519 (MLR) and stepwise MLR, using consistent out-of-sample cross-validation methods. When considering local meteorological
520 factors only, RFR outperforms the linear approaches RR and MLR, which in turn perform better than stepwise MLR that uses
521 the only the three locally most significant meteorological factors. A major advantage of RFR is its ability to model non-linear
522 relationships (e.g., often observed between temperature and ozone). In addition, we tested how the consideration of larger scale
523 meteorological controlling factors improves our predictive performance. MLR noticeably suffers from the “curse of
524 dimensionality” due to the large increase of the number of predictors when we included additional meteorological information
525 spanning a 7.5°×7.5° domain around the target grid point for ozone pollution. In contrast, RR can deal well with this increase
526 in the number of predictors subject to an objective cross-validation approach for its hyperparameter tuning. In particular,
527 despite not directly considering non-linearity, we find an improvement of model performance in RR with additional 2-
528 dimensional predictors, which outperforms RFR with only local meteorological predictors in southern China, indicating the
529 importance of considering a wider meteorological context in future controlling factor analyses of this kind.

530 A key advantage of our approach is that both RFR and RR allow for a straightforward interpretation of the predictive
531 models. Reassuringly, we find a good agreement regarding the identification of the dominant local meteorological drivers for



532 each region. In general, ozone pollution in northern China such as in the Beijing-Tianjin-Hebei (BTH) region is predominantly
533 driven by temperature fluctuations while ozone in southern China like in Pearl River Delta (PRD) region is particularly strongly
534 controlled by humidity, possibly due to the important role of humid weather in preventing significant ozone pollution episodes
535 in this region, while the effect of humidity is constrained in BTH probably because of the relatively drier condition in this
536 region. Besides, we observe a strong influence in PRD of air exchange with pristine marine regions, leading to a greater
537 influence of large-scale wind directions, e.g., through the transport of clean marine air into the region, or through air stagnation
538 and ozone accumulation under large-scale sinking atmospheric motion. Surface solar radiation plays a major role in general
539 due to its importance for setting the conditions for ozone photochemistry, which is particularly dominant in the Yangtze River
540 Delta (YRD) and Sichuan Basin. Our work thus highlights that surface solar radiation might be a key predictor to consider in
541 future controlling factor analyses in these two regions. In summary, hot, dry and sunny weather tends to provide more favorable
542 conditions for ozone pollution in China, which is not entirely unexpected but carries important implications for future changes
543 in air pollution under climate change, while simultaneously considering the pivotal role of targeted emission control strategies
544 on ozone precursors.

545 In terms of ozone trends, we find a linear MDA8 ozone increase of about 1.1 ppbv a⁻¹ on average during April to October
546 from 2015 to 2019 across China. Regionally, these trends can be more than twice as large as in BTH. The largest positive
547 trends may be mostly attributed to non-meteorological factors such as change of precursors' emissions. However,
548 meteorologically driven trends on average shows increases at 0.5 ppbv a⁻¹ across China, equalling almost 50% over the period
549 considered here, and it is thus estimated to be more important factor, especially in southern China and the YRD region. While
550 the effect of meteorology might generally hinder extreme ozone pollution in the Sichuan Basin region, we conclude that
551 maintaining continuous emission control strategies is preferable in case of the occurrence of unfavorable weather conditions
552 for ozone mitigation.

553 **Data/Code availability**

554 The original air quality data including hourly and 8-hour rolling mean of ozone are available at <https://quotsoft.net/air/>
555 (Wang, X. L., 2021; last accessed: 13 July 2021). The ERA5 reanalysis product is available at
556 <https://cds.climate.copernicus.eu/> (last accessed: 11 November 2021). The codes for machine learning algorithms are available
557 from the corresponding author upon request.

558 **Author contribution**

559 P.N., X.W. and G.F. designed the study. X.W. performed the modelling and analysis of the data, supervised by P.N. and
560 G.F. X.W. wrote the paper with input and revision from P.N. and G.F.



561 **Competing interests**

562 The authors declare that they have no conflict of interest.

563 **References**

- 564 Archibald, A. T., Turnock, S. T., Griffiths, P. T., Cox, T., Derwent, R. G., Knote, C., and Shin, M.: On the changes in
565 surface ozone over the twenty-first century: sensitivity to changes in surface temperature and chemical mechanisms:
566 21st century changes in surface ozone, *Philos. Trans. R. Soc. A Math. Phys. Eng. Sci.*, 378,
567 <https://doi.org/10.1098/rsta.2019.0329>, 2020.
- 568 Bishop, C. M.: Pattern recognition and machine learning, Springer Science+Business Media, Singapore, 2006.
- 569 Breiman, L.: Random Forests, *Mach. Learn.*, <https://doi.org/10.1023/A:1010933404324>, 2001.
- 570 Ceppi, P. and Nowack, P.: Observational evidence that cloud feedback amplifies global warming, *Proc. Natl. Acad. Sci. U.*
571 *S. A.*, 118, 1–7, <https://doi.org/10.1073/pnas.2026290118>, 2021.
- 572 Chang, L., Xu, J., Tie, X., and Gao, W.: The impact of Climate Change on the Western Pacific Subtropical High and the
573 related ozone pollution in Shanghai, China, *Sci. Rep.*, 9, 1–12, <https://doi.org/10.1038/s41598-019-53103-7>, 2019.
- 574 Chen, X., Jiang, Z., Shen, Y., Li, R., Fu, Y., Liu, J., Han, H., Liao, H., Cheng, X., Jones, D. B. A., Worden, H., and Abad, G.
575 G.: Chinese Regulations Are Working—Why Is Surface Ozone Over Industrialized Areas Still High? Applying Lessons
576 From Northeast US Air Quality Evolution, *Geophys. Res. Lett.*, 48, <https://doi.org/10.1029/2021GL092816>, 2021.
- 577 Chen, Z., Liu, J., Cheng, X., Yang, M., and Wang, H.: Positive and negative influences of landfalling typhoons on
578 tropospheric ozone over southern China, *Atmos. Chem. Phys. Discuss.*, 1–22, <https://doi.org/10.5194/acp-2021-573>,
579 2021.
- 580 Chinese State Council: Action Plan on Air Pollution Prevention and Control (in Chinese), available at:
581 http://www.gov.cn/zwqk/2013-09/12/content_2486773.htm (last access: 24 November 2021), 2013.
- 582 Ding, Y. and Chan, J. C. L.: The East Asian summer monsoon: An overview, *Meteorol. Atmos. Phys.*, 89, 117–142,
583 <https://doi.org/10.1007/s00703-005-0125-z>, 2005.
- 584 Doherty, R. M., Wild, O., Shindell, D. T., Zeng, G., MacKenzie, I. A., Collins, W. J., Fiore, A. M., Stevenson, D. S.,
585 Dentener, F. J., Schultz, M. G., Hess, P., Derwent, R. G., and Keating, T. J.: Impacts of climate change on surface
586 ozone and intercontinental ozone pollution: A multi-model study, *J. Geophys. Res. Atmos.*, 118, 3744–3763,
587 <https://doi.org/10.1002/jgrd.50266>, 2013.
- 588 Dormann, C. F., Elith, J., Bacher, S., Buchmann, C., Carl, G., Carré, G., Marquéz, J. R. G., Gruber, B., Lafourcade, B.,
589 Leitão, P. J., Münkemüller, T., McClean, C., Osborne, P. E., Reineking, B., Schröder, B., Skidmore, A. K., Zurell, D.,
590 and Lautenbach, S.: Collinearity: A review of methods to deal with it and a simulation study evaluating their
591 performance, *Ecography.*, 36, 27–46, <https://doi.org/10.1111/j.1600-0587.2012.07348.x>, 2013.
- 592 Finlayson-Pitts, B. and Pitts, J.: Chemistry of the upper and lower atmosphere, Academic Press, San Diego, 2000.



- 593 Gao, M., Gao, J., Zhu, B., Kumar, R., Lu, X., Song, S., Zhang, Y., Jia, B., Wang, P., Beig, G., Hu, J., Ying, Q., Zhang, H.,
594 Sherman, P., and B. McElroy, M.: Ozone pollution over china and india: Seasonality and sources, *Atmos. Chem. Phys.*,
595 20, 4399–4414, <https://doi.org/10.5194/acp-20-4399-2020>, 2020.
- 596 Grange, S. K., Carslaw, D. C., Lewis, A. C., Boleti, E., and Hueglin, C.: Random forest meteorological normalisation
597 models for Swiss PM10 trend analysis, *Atmos. Chem. Phys.*, 18, 6223–6239, <https://doi.org/10.5194/acp-18-6223->
598 2018, 2018.
- 599 Gu, Y., Li, K., Xu, J., Liao, H., and Zhou, G.: Observed dependence of surface ozone on increasing temperature in Shanghai,
600 China, *Atmos. Environ.*, 221, <https://doi.org/10.1016/j.atmosenv.2019.117108>, 2020.
- 601 Guenther, A. B., Zimmerman, P. R., Harley, P. C., Monson, R. K., and Fall, R.: Isoprene and monoterpene emission rate
602 variability: model evaluations and sensitivity analyses, *J. Geophys. Res.*, 98, <https://doi.org/10.1029/93jd00527>, 1993.
- 603 Han, H., Liu, J., Shu, L., Wang, T., and Yuan, H.: Local and synoptic meteorological influences on daily variability in
604 summertime surface ozone in eastern China, *Atmos. Chem. Phys.*, 20, 203–222, <https://doi.org/10.5194/acp-20-203->
605 2020, 2020.
- 606 Hersbach, H., Bell, B., Berrisford, P., Hirahara, S., Horányi, A., Muñoz-Sabater, J., Nicolas, J., Peubey, C., Radu, R.,
607 Schepers, D., Simmons, A., Soci, C., Abdalla, S., Abellan, X., Balsamo, G., Bechtold, P., Biavati, G., Bidlot, J.,
608 Bonavita, M., De Chiara, G., Dahlgren, P., Dee, D., Diamantakis, M., Dragani, R., Flemming, J., Forbes, R., Fuentes,
609 M., Geer, A., Haimberger, L., Healy, S., Hogan, R. J., Hólm, E., Janisková, M., Keeley, S., Laloyaux, P., Lopez, P.,
610 Lupu, C., Radnoti, G., de Rosnay, P., Rozum, I., Vamborg, F., Villaume, S., and Thépaut, J. N.: The ERA5 global
611 reanalysis, *Q. J. R. Meteorol. Soc.*, 146, 1999–2049, <https://doi.org/10.1002/qj.3803>, 2020.
- 612 Hua, W., Chen, Z. M., Jie, C. Y., Kondo, Y., Hofzumahaus, A., Takegawa, N., Chang, C. C., Lu, K. D., Miyazaki, Y., Kita,
613 K., Wang, H. L., Zhang, Y. H., and Hu, M.: Atmospheric hydrogen peroxide and organic hydroperoxides during
614 PRIDE-PRD'06, China: Their concentration, formation mechanism and contribution to secondary aerosols, *Atmos.*
615 *Chem. Phys.*, 8, 6755–6773, <https://doi.org/10.5194/acp-8-6755-2008>, 2008.
- 616 Jacob, D. J.: Heterogeneous chemistry and tropospheric ozone, *Atmos. Environ.*, 34, 2131–2159,
617 [https://doi.org/10.1016/S1352-2310\(99\)00462-8](https://doi.org/10.1016/S1352-2310(99)00462-8), 2000.
- 618 Jiang, Y. C., Zhao, T. L., Liu, J., Xu, X. D., Tan, C. H., Cheng, X. H., Bi, X. Y., Gan, J. B., You, J. F., and Zhao, S. Z.: Why
619 does surface ozone peak before a typhoon landing in southeast China?, *Atmos. Chem. Phys.*, 15, 13331–13338,
620 <https://doi.org/10.5194/acp-15-13331-2015>, 2015.
- 621 Kuhn-Régner, A., Voulgarakis, A., Nowack, P., Forkel, M., Prentice, I. C., and Harrison, S. P.: The importance of
622 antecedent vegetation and drought conditions as global drivers of burnt area, 18, 3861–3879, <https://doi.org/10.5194/bg->
623 18-3861-2021, 2021.
- 624 Lefohn, A. S., Malley, C. S., Smith, L., Wells, B., Hazucha, M., Simon, H., Naik, V., Mills, G., Schultz, M. G., Paoletti, E.,
625 De Marco, A., Xu, X., Zhang, L., Wang, T., Neufeld, H. S., Musselman, R. C., Tarasick, D., Brauer, M., Feng, Z.,



- 626 Tang, H., Kobayashi, K., Sicard, P., Solberg, S., and Gerosa, G.: Tropospheric ozone assessment report: Global ozone
627 metrics for climate change, human health, and crop/ecosystem research, 6, <https://doi.org/10.1525/elementa.279>, 2018.
- 628 Lelieveld, J., Evans, J. S., Fnais, M., Giannadaki, D., and Pozzer, A.: The contribution of outdoor air pollution sources to
629 premature mortality on a global scale, *Nature*, 525, 367–371, <https://doi.org/10.1038/nature15371>, 2015.
- 630 Li, K., Chen, L., Ying, F., White, S. J., Jang, C., Wu, X., Gao, X., Hong, S., Shen, J., Azzi, M., and Cen, K.: Meteorological
631 and chemical impacts on ozone formation: A case study in Hangzhou, China, *Atmos. Res.*, 196, 40–52,
632 <https://doi.org/10.1016/j.atmosres.2017.06.003>, 2017.
- 633 Li, K., Jacob, D. J., Liao, H., Shen, L., Zhang, Q., and Bates, K. H.: Anthropogenic drivers of 2013–2017 trends in summer
634 surface ozone in China, *Proc. Natl. Acad. Sci. U. S. A.*, 116, 422–427, <https://doi.org/10.1073/pnas.1812168116>, 2019a.
- 635 Li, K., Jacob, D. J., Liao, H., Zhu, J., Shah, V., Shen, L., Bates, K. H., Zhang, Q., and Zhai, S.: A two-pollutant strategy for
636 improving ozone and particulate air quality in China, *Nat. Geosci.*, 12, 906–910, <https://doi.org/10.1038/s41561-019-0464-x>, 2019b.
- 638 Li, K., Jacob, D. J., Shen, L., Lu, X., De Smedt, I., and Liao, H.: Increases in surface ozone pollution in China from 2013 to
639 2019: Anthropogenic and meteorological influences, *Atmos. Chem. Phys.*, 20, 11423–11433,
640 <https://doi.org/10.5194/acp-20-11423-2020>, 2020.
- 641 Liu, Y. and Wang, T.: Worsening urban ozone pollution in China from 2013 to 2017 - Part 2: The effects of emission
642 changes and implications for multi-pollutant control, *Atmos. Chem. Phys.*, 20, 6323–6337, <https://doi.org/10.5194/acp-20-6323-2020>, 2020.
- 644 Lu, X., Zhang, L., and Shen, L.: Meteorology and Climate Influences on Tropospheric Ozone: a Review of Natural Sources,
645 Chemistry, and Transport Patterns, *Curr. Pollut. Reports*, 5, 238–260, <https://doi.org/10.1007/s40726-019-00118-3>,
646 2019a.
- 647 Lu, X., Zhang, L., Chen, Y., Zhou, M., Zheng, B., Li, K., Liu, Y., Lin, J., Fu, T. M., and Zhang, Q.: Exploring 2016–2017
648 surface ozone pollution over China: Source contributions and meteorological influences, *Atmos. Chem. Phys.*, 19,
649 8339–8361, <https://doi.org/10.5194/acp-19-8339-2019>, 2019b.
- 650 Ma, M., Gao, Y., Wang, Y., Zhang, S., Ruby Leung, L., Liu, C., Wang, S., Zhao, B., Chang, X., Su, H., Zhang, T., Sheng,
651 L., Yao, X., and Gao, H.: Substantial ozone enhancement over the North China Plain from increased biogenic emissions
652 due to heat waves and land cover in summer 2017, *Atmos. Chem. Phys.*, 19, 12195–12207, <https://doi.org/10.5194/acp-19-12195-2019>, 2019.
- 654 Mansfield, L. A., Nowack, P. J., Kasoar, M., Everitt, R. G., Collins, W. J., and Voulgarakis, A.: Predicting global patterns of
655 long-term climate change from short-term simulations using machine learning, *npj Clim. Atmos. Sci.*, 3,
656 <https://doi.org/10.1038/s41612-020-00148-5>, 2020.
- 657 McDonald, G. C.: Ridge regression, *Wiley Interdiscip. Rev. Comput. Stat.*, 1, 93–100, <https://doi.org/10.1002/wics.14>, 2009.
- 658 Meehl, G. A., Tebaldi, C., Tilmes, S., Lamarque, J. F., Bates, S., Pendergrass, A., and Lombardozzi, D.: Future heat waves
659 and surface ozone, *Environ. Res. Lett.*, 13, <https://doi.org/10.1088/1748-9326/aabdc>, 2018.



- 660 Menze, B. H., Kelm, B. M., Masuch, R., Himmelreich, U., Bachert, P., Petrich, W., and Hamprecht, F. A.: A comparison of
661 random forest and its Gini importance with standard chemometric methods for the feature selection and classification of
662 spectral data, *BMC Bioinformatics*, 10, 1–16, <https://doi.org/10.1186/1471-2105-10-213>, 2009.
- 663 MEP: Ministry of Environmental Protection of the People’s Republic of China, Ambient Air Quality Standards (GB3095-
664 2012) (In Chinese), 2012.
- 665 Monks, P. S., Archibald, A. T., Colette, A., Cooper, O., Coyle, M., Derwent, R., Fowler, D., Granier, C., Law, K. S., Mills,
666 G. E., Stevenson, D. S., Tarasova, O., Thouret, V., Von Schneidemesser, E., Sommariva, R., Wild, O., and Williams,
667 M. L.: Tropospheric ozone and its precursors from the urban to the global scale from air quality to short-lived climate
668 forcer, *Atmos. Chem. Phys.*, 15, 8889–8973, <https://doi.org/10.5194/acp-15-8889-2015>, 2015.
- 669 Ning, G., Yim, S. H. L., Yang, Y., Gu, Y., and Dong, G.: Modulations of synoptic and climatic changes on ozone pollution
670 and its health risks in mountain-basin areas, *Atmos. Environ.*, 240, 117808,
671 <https://doi.org/10.1016/j.atmosenv.2020.117808>, 2020.
- 672 Nowack, P., Braesicke, P., Haigh, J., Abraham, N. L., Pyle, J., and Voulgarakis, A.: Using machine learning to build
673 temperature-based ozone parameterizations for climate sensitivity simulations, *Environ. Res. Lett.*, 13,
674 <https://doi.org/10.1088/1748-9326/aae2be>, 2018.
- 675 Nowack, P., Konstantinovskiy, L., Gardiner, H., and Cant, J.: Machine learning calibration of low-cost NO₂ and PM₁₀
676 sensors: Non-linear algorithms and their impact on site transferability, *Atmos. Meas. Tech.*, 14, 5637–5655,
677 <https://doi.org/10.5194/amt-14-5637-2021>, 2021.
- 678 Otero, N., Sillmann, J., Mar, K. A., Rust, H. W., Solberg, S., Andersson, C., Engardt, M., Bergström, R., Bessagnet, B.,
679 Colette, A., Couvidat, F., Cuvelier, C., Tsyro, S., Fagerli, H., Schaap, M., Manders, A., Mircea, M., Briganti, G.,
680 Cappelletti, A., Adani, M., D’Isidoro, M., Pay, M. T., Theobald, M., Vivanco, M. G., Wind, P., Ojha, N., Raffort, V.,
681 and Butler, T.: A multi-model comparison of meteorological drivers of surface ozone over Europe, *Atmos. Chem.*
682 *Phys.*, 18, 12269–12288, <https://doi.org/10.5194/acp-18-12269-2018>, 2018.
- 683 Ou, J., Yuan, Z., Zheng, J., Huang, Z., Shao, M., Li, Z., Huang, X., Guo, H., and Louie, P. K. K.: Ambient Ozone Control in
684 a Photochemically Active Region: Short-Term Despiking or Long-Term Attainment?, *Environ. Sci. Technol.*, 50,
685 5720–5728, <https://doi.org/10.1021/acs.est.6b00345>, 2016.
- 686 Pu, X., Wang, T. J., Huang, X., Melas, D., Zanis, P., Papanastasiou, D. K., and Poupkou, A.: Enhanced surface ozone during
687 the heat wave of 2013 in Yangtze River Delta region, China, *Sci. Total Environ.*, 603–604, 807–816,
688 <https://doi.org/10.1016/j.scitotenv.2017.03.056>, 2017.
- 689 Qi, J., Zheng, B., Li, M., Yu, F., Chen, C., Liu, F., Zhou, X., Yuan, J., Zhang, Q., and He, K.: A high-resolution air
690 pollutants emission inventory in 2013 for the Beijing-Tianjin-Hebei region, China, *Atmos. Environ.*, 170, 156–168,
691 <https://doi.org/10.1016/j.atmosenv.2017.09.039>, 2017.



- 692 Qu, K., Wang, X., Yan, Y., Shen, J., Xiao, T., Dong, H., Zeng, L., and Zhang, Y.: A comparative study to reveal the
693 influence of typhoons on the transport, production and accumulation of O₃ in the Pearl River Delta, China, *Atmos.*
694 *Chem. Phys.*, 21, 11593–11612, <https://doi.org/10.5194/acp-21-11593-2021>, 2021.
- 695 Shu, L., Wang, T., Han, H., Xie, M., Chen, P., Li, M., and Wu, H.: Summertime ozone pollution in the Yangtze River Delta
696 of eastern China during 2013–2017: Synoptic impacts and source apportionment, *Environ. Pollut.*, 257, 113631,
697 <https://doi.org/10.1016/j.envpol.2019.113631>, 2020.
- 698 Shu, L., Xie, M., Wang, T., Gao, D., Chen, P., Han, Y., Li, S., Zhuang, B., and Li, M.: Integrated studies of a regional ozone
699 pollution synthetically affected by subtropical high and typhoon system in the Yangtze River Delta region, China,
700 *Atmos. Chem. Phys.*, 16, 15801–15819, <https://doi.org/10.5194/acp-16-15801-2016>, 2016.
- 701 Sillman, S.: The relation between ozone, NO_x and hydrocarbons in urban and polluted rural environments, *Atmos. Environ.*,
702 [https://doi.org/10.1016/S1352-2310\(98\)00345-8](https://doi.org/10.1016/S1352-2310(98)00345-8), 1999.
- 703 So, K. L. and Wang, T.: On the local and regional influence on ground-level ozone concentrations in Hong Kong, *Environ.*
704 *Pollut.*, 123, 307–317, [https://doi.org/10.1016/S0269-7491\(02\)00370-6](https://doi.org/10.1016/S0269-7491(02)00370-6), 2003.
- 705 Song, C., Liu, B., Dai, Q., Li, H., and Mao, H.: Temperature dependence and source apportionment of volatile organic
706 compounds (VOCs) at an urban site on the north China plain, *Atmos. Environ.*, 207, 167–181,
707 <https://doi.org/10.1016/j.atmosenv.2019.03.030>, 2019.
- 708 Squire, O. J., Archibald, A. T., Griffiths, P. T., Jenkin, M. E., Smith, D., and Pyle, J. A.: Influence of isoprene chemical
709 mechanism on modelled changes in tropospheric ozone due to climate and land use over the 21st century, *Atmos.*
710 *Chem. Phys.*, 15, 5123–5143, <https://doi.org/10.5194/acp-15-5123-2015>, 2015.
- 711 Stirnberg, R., Cermak, J., Kotthaus, S., Haefelin, M., Andersen, H., Fuchs, J., Kim, M., Petit, J. E., and Favez, O.:
712 Meteorology-driven variability of air pollution (PM₁) revealed with explainable machine learning, *Atmos. Chem. Phys.*,
713 21, 3919–3948, <https://doi.org/10.5194/acp-21-3919-2021>, 2021.
- 714 Wang, H., Wu, K., Liu, Y., Sheng, B., Lu, X., He, Y., Xie, J., Wang, H., and Fan, S.: Role of Heat Wave-Induced Biogenic
715 VOC Enhancements in Persistent Ozone Episodes Formation in Pearl River Delta, *J. Geophys. Res. Atmos.*, 126, 1–19,
716 <https://doi.org/10.1029/2020JD034317>, 2021.
- 717 Wang, N., Lyu, X., Deng, X., Huang, X., Jiang, F., and Ding, A.: Aggravating O₃ pollution due to NO_x emission control in
718 eastern China, *Sci. Total Environ.*, 677, 732–744, <https://doi.org/10.1016/j.scitotenv.2019.04.388>, 2019.
- 719 Wang, T., Xue, L., Brimblecombe, P., Lam, Y. F., Li, L., and Zhang, L.: Ozone pollution in China: A review of
720 concentrations, meteorological influences, chemical precursors, and effects, *Sci. Total Environ.*, 575, 1582–1596,
721 <https://doi.org/10.1016/j.scitotenv.2016.10.081>, 2017.
- 722 Wang, X. L.: Historical air quality data in China, available at: <https://quotsoft.net/air>, last access: 13 July 2021.
- 723 Wang, Y., Shen, L., Wu, S., Mickley, L., He, J., and Hao, J.: Sensitivity of surface ozone over China to 2000–2050 global
724 changes of climate and emissions, *Atmos. Environ.*, 75, 374–382, <https://doi.org/10.1016/j.atmosenv.2013.04.045>,
725 2013.



- 726 Wei, X., Lam, K. S., Cao, C., Li, H., and He, J.: Dynamics of the Typhoon Haitang Related High Ozone Episode over Hong
727 Kong, *Adv. Meteorol.*, 2016, <https://doi.org/10.1155/2016/6089154>, 2016.
- 728 Xie, X., Shao, M., Liu, Y., Lu, S., Chang, C. C., and Chen, Z. M.: Estimate of initial isoprene contribution to ozone
729 formation potential in Beijing, China, *Atmos. Environ.*, 42, 6000–6010,
730 <https://doi.org/10.1016/j.atmosenv.2008.03.035>, 2008.
- 731 Yang, L., Xie, D., Yuan, Z., Huang, Z., Wu, H., Han, J., Liu, L., and Jia, W.: Quantification of regional ozone pollution
732 characteristics and its temporal evolution: Insights from identification of the impacts of meteorological conditions and
733 emissions, *Atmosphere.*, 12, <https://doi.org/10.3390/atmos12020279>, 2021.
- 734 Young, P. J., Archibald, A. T., Bowman, K. W., Lamarque, J.-F., Naik, V., Stevenson, D. S., Tilmes, S., Voulgarakis, A.,
735 Wild, O., Bergmann, D., Cameron-Smith, P., Cionni, I., Collins, W. J., Dalsøren, S. B., Doherty, R. M., Eyring, V.,
736 Faluvegi, G., Horowitz, L. W., Josse, B., Lee, Y. H., MacKenzie, I. A., Nagashima, T., Plummer, D. A., Righi, M.,
737 Rumbold, S. T., Skeie, R. B., Shindell, D. T., Strode, S. A., Sudo, K., Szopa, S., and Zeng, G.: Pre-industrial to end 21st
738 century projections of tropospheric ozone from the Atmospheric Chemistry and Climate Model Intercomparison Project
739 (ACCMIP), *Atmos. Chem. Phys.*, 13, 2063–2090, <https://doi.org/10.5194/acp-13-2063-2013>, 2013.
- 740 Zhai, S., Jacob, D. J., Wang, X., Shen, L., Li, K., Zhang, Y., Gui, K., Zhao, T., and Liao, H.: Fine particulate matter (PM_{2.5})
741 trends in China, 2013–2018. separating contributions from anthropogenic emissions and meteorology, *Atmos. Chem.*
742 *Phys.*, 19, 11031–11041, <https://doi.org/10.5194/acp-19-11031-2019>, 2019.
- 743 Zhang, J., Gao, Y., Luo, K., Ruby Leung, L., Zhang, Y., Wang, K., and Fan, J.: Impacts of compound extreme weather
744 events on ozone in the present and future, *Atmos. Chem. Phys.*, 18, 9861–9877, [https://doi.org/10.5194/acp-18-9861-](https://doi.org/10.5194/acp-18-9861-2018)
745 2018, 2018.
- 746 Zhang, W., Zou, Y., Zheng, X. D., Wang, N., Yan, H., Chen, Y. P., Zhao, X. J., Ji, Z. P., Li, F., Mai, B. R., Yin, C. Q., Deng,
747 T., Fan, L. Y., and Deng, X. J.: Characteristics of the vertical distribution of tropospheric ozone in late autumn at
748 Yangjiang station in Pearl River Delta (PRD), China. Part I: Observed event, *Atmos. Environ.*, 244,
749 <https://doi.org/10.1016/j.atmosenv.2020.117898>, 2021.
- 750 Zhang, X., Fung, J. C. H., Lau, A. K. H., Hossain, M. S., Louie, P. K. K., and Huang, W.: Air quality and synergistic health
751 effects of ozone and nitrogen oxides in response to China’s integrated air quality control policies during 2015–2019,
752 *Chemosphere*, 268, 129385, <https://doi.org/10.1016/j.chemosphere.2020.129385>, 2021.
- 753 Zhao, X., Yu, B., Liu, Y., Chen, Z., Li, Q., Wang, C., and Wu, J.: Estimation of poverty using random forest regression with
754 multi-source data: A case study in Bangladesh, *Remote Sens.*, 11, 1–18, <https://doi.org/10.3390/rs11040375>, 2019.
- 755 Zheng, B., Tong, D., Li, M., Liu, F., Hong, C., Geng, G., Li, H., Li, X., Peng, L., Qi, J., Yan, L., Zhang, Y., Zhao, H., Zheng,
756 Y., He, K., and Zhang, Q.: Trends in China’s anthropogenic emissions since 2010 as the consequence of clean air
757 actions, *Atmos. Chem. Phys.*, 18, 14095–14111, <https://doi.org/10.5194/acp-18-14095-2018>, 2018.
- 758 Zhou, T. J. and Yu, R. C.: Atmospheric water vapor transport associated with typical anomalous summer rainfall patterns in
759 China, *J. Geophys. Res. D Atmos.*, 110, 1–10, <https://doi.org/10.1029/2004JD005413>, 2005.